

Capacitive and kinetic characteristics of Ru-Ti oxide electrodes: influence of variation in the Ru content

B.V. Tilak, C.-P. Chen, V.I. Birss, and J. Wang

Abstract: A systematic investigation has been carried out of thermally formed Ru-Ti oxide electrodes of varying Ru content, correlating their voltammetric and impedance characteristics in NaCl solutions with the kinetics of the chlorine evolution reaction. The Tafel slope increases markedly with lower Ru content (< ca. 25 at.%), indicative either of the contribution of increasing oxide resistance or of a change in mechanism. The exchange current density is linearly proportional to the Ru content down to <10 at.% Ru, below which the film appears to respond more like a highly resistive film material. The film resistance and capacitance, determined by equivalent circuit fitting in the absence of dissolved chlorine, were used to calculate the expected impedance response of the oxide film, based on a model of an activation-controlled surface redox reaction occurring in a porous matrix. The calculated results show the dominant signature of the matrix resistance at low Ru loadings, in both the phase angle impedance data and in the Tafel plots, in agreement with the experimental observations.

Key words: Ru oxide, Ru-Ti oxide, chlorine evolution, kinetics, capacitance, equivalent circuit, impedance, Tafel data.

Résumé : On a effectué une étude systématique d'électrodes de l'oxyde de Ru-Ti, formées thermiquement, contenant diverses quantités de Ru; on a établi une corrélation entre leurs caractéristiques voltampérométriques et d'impédance dans des solutions de NaCl avec la cinétique de la réaction d'évolution du chlore. La pente de Tafel augmente d'une façon importante aux faibles concentrations de Ru (inférieures à environ 25 at.%); ceci suggère une augmentation de contribution de la résistance de l'oxyde ou un changement de mécanisme. La densité du courant d'échange est linéairement proportionnelle à la concentration du Ru jusqu'à des valeurs inférieures à 10 at.% de Ru; en dessous de ces valeurs, le film semble répondre plus comme un film ayant une grande résistivité. On a utilisé la résistance et la capacitance du film, déterminées par un ajustement de circuit équivalent en l'absence de chlore dissous, pour calculer la réponse attendue de l'impédance de l'oxyde de film; à cette fin, on a fait appel à un modèle de réaction redox de surface contrôlée par l'activation et se produisant dans une matrice poreuse. Les résultats calculés montrent que la signature dominante de la résistance de la matrice à de faibles doses de Ru est en accord avec les données expérimentales, tant pour les données d'impédance que pour les courbes de Tafel.

Mots clés : oxyde de ruthénium, oxyde de Ru-Ti, évolution de chlore, cinétique, capacitance, circuit équivalent, impédance, données de Tafel.

[Traduit par la rédaction]

1.0 Introduction

Understanding the electrochemical properties of thermally formed Ru-Ti oxide electrodes, commonly used as anodes in the chlor-alkali industry, is very important in order to forecast, and to enable the optimization of, their overall performance during chlorine evolution in industrial operations. Extensive prior investigations have been directed towards understanding

Ru-Ti oxide electrode characteristics and to establishing the relationship between their structural and electrical properties and their Ru content. Several comprehensive and critical analyses of these prior results have been presented previously (1-3).

The effect of the temperature employed during the formation of Ru-Ti oxides on their structure has been examined (4-6), and it was reported that the oxide obtained at 400°C is a metastable solid solution, while a crystalline mixture is obtained at 700-800°C. Spasskaya et al. (7) concluded that the change of the roughness factor (200 to 800) that occurs with composition has little effect on the oxide surface properties. It was also reported by various groups (5-9) that the resistance of Ru-Ti oxide films increases sharply with decreasing Ru content for films containing less than ca. 25 at.% Ru (7, 8).

Doblhofer et al. (10) studied the effect of sweep rate on the charge passed in cyclic voltammetry (CV) experiments by thermally formed Ru-Ti oxide electrodes, allowing the diffusion coefficients to be estimated. A study of the effect of the Ru composition on the CV charge of the Ru-Ti oxide electrodes (6, 11-13) showed that it could be used to measure their

Received June 10, 1997.

This paper is dedicated to Dr. Brian E. Conway, in honour of his many scientific contributions and on the occasion of his 70th birthday.

B.V. Tilak and C.-P. Chen. Occidental Chemical Corporation, Technology Centre, Grand Island, NY 14072, U.S.A.
V.I. Birss¹ and J. Wang. Department of Chemistry, University of Calgary, Calgary, AB T2N 1N4, Canada.

¹ Author to whom correspondence may be addressed.
Telephone: (403) 220-6432. Fax: (403) 289-9488. E-mail: birss@acs.ucalgary.ca

true surface area. Shieh and Hwang (14) studied the electrochemical behavior of Ru–Ti oxide electrodes doped with small amounts of Sn and found the relationship between the CV charge and the double layer capacity (obtained from ac impedance experiments) to be linear and also that the capacity could yield the electrochemically active surface area. Investigations of the influence of temperature on the CV response (13, 15, 16) revealed the Arrhenius relation to be obeyed, yielding an activation enthalpy of ca. 4–5 kJ/mol.

Vallet et al. (17, 18) studied the properties of ion-implanted Ru- and Ir–Ti electrodes and found the electrochemical activity of Ru-implanted electrodes to be 2 to 3 times higher than that of the Ir-implanted ones, while the corrosion rate of the latter was only ca. 1% of the former. They also reported that the mechanism of electrical conductance of these oxides changes from semiconducting to metallic when a surface Ru concentration of 2.6×10^{21} atoms cm^{-3} is exceeded, corresponding to about 25 at.% Ru in the Ru–Ti oxide film.

Most of the investigations performed in the past with thermally formed Ru–Ti oxide electrodes have focussed on the kinetics of the chlorine evolution reaction on these oxide surfaces. However, no systematic studies have to date been reported relating the electrochemical and impedance properties of these metal oxide electrodes, under conditions when only the oxide film is redox-active, to the kinetic characteristics of these materials in the faradaic domain of the chlorine evolution reaction. In the present paper, attempts have been made to explain the changes in the chlorine evolution Tafel data, in terms of the combined effect of changing film resistivity and of the density of active Ru sites, with the change in the Ru content of the films. This study was also considered relevant in terms of attempting to further the understanding of the origin of the problematic loss of kinetic activity, seen with some Ru–Ti oxide anodes, in practice.

2.0 Experimental

The working electrode substrate consisted of 99.99% Ti wire of 2 mm diameter, purchased from Johnson Matthey, Inc. The cross-sectional end (0.0314 cm^2) of each fresh titanium wire electrode was first polished with 600 grit emery paper, and then dipped in hot oxalic acid (1.25 mol/L) + 2.2 mol/L hydrochloric acid to remove the air-formed oxide film from the surface. It was then rinsed with acetone, dried, rinsed with methylene chloride, dried again, and then rinsed with triply distilled water.

Ruthenium(III) chloride (18.2 g, Johnson Matthey & Mallory Ltd.), titanium(VI) butoxide (45 ml, Aldrich Chemical Co. Inc.), and 4.4 mol/L hydrochloric acid (6 mL) were mixed together to make the coating solution.² The Ti wire electrodes were then painted with a thin layer of this solution and allowed to air-dry. A single coat under normal conditions yielded a coating thickness, estimated by its weight gain, to be ca. 2 μm . In other experiments, a thinner film of 0.6–0.7 μm thickness was deposited in two coats from a 5 \times diluted Ru–Ti coating solution. These coatings were then converted to the oxide by heating at a rate of 5°C/min to 100°C, and then remaining at 100°C for 15 min to remove the solvent. The tem-

perature was then increased at 10°C/min to 440°C in air and maintained at 440°C for 30 min to decompose the Ru–Ti compounds into the corresponding oxides. Afterwards, the side of each oxide-coated Ti wire was insulated with Teflon tape, leaving only the cross-sectional end to serve as the working electrode (WE) in the NaCl test solution.

All experiments were carried out in 5 mol/L NaCl (EM Science) made up with triply distilled water. The pH of the NaCl solution was adjusted both before and during electrolysis to ca. 4 by the addition of either 0.5 or 2 mol/L HCl at regular intervals. All electrolysis experiments were carried out without additional stirring of the solution or removal of the dissolved oxygen, in a one-compartment cell at both room temperature (20–22°C) and at 90°C. IR compensation was employed for the Tafel analysis of the chlorine evolution data in all of the experiments.

The counter electrode (CE) was a 40 at.% Ru oxide coating on a Ti substrate, of more than 100 times the apparent surface area of the WE. It was positioned inside a Teflon tube to minimize the amount of hydrogen gas that passed into the solution in the main compartment. An Ag/AgCl electrode was employed as the reference electrode (RE) at high temperatures, while an SCE generally served as the RE at room temperature. All potentials are given versus the SCE in this paper.

An EG&G PAR 273 potentiostat/galvanostat was used in all electrolysis and CV experiments, with the data plotted on an HP 7044B X-Y recorder. A Solartron 1255 HF frequency response analyzer, coupled with a Solartron 1286 electrochemical interface, was employed for the ac impedance measurements, using frequencies from 0.1 to 65 kHz and a 10 mV rms amplitude (effective) applied at the open circuit potential (OCP). As the SCE reference electrode introduces a time delay to the potentiostat, seen as a phase shift at high frequencies due to its resistance and capacitance characteristics, an additional Pt wire electrode was placed in the cell and was connected via a 6.8 μF capacitor to the RE lead (19–21). Data acquisition was carried out using Z-Plot software (Scribner Associates) and its evaluation was achieved using a nonlinear least-squares fit program (Equivalent Circuit, Version 3.97, written by B. Boukamp, University of Twente).

3.0 Results and discussion

3.1 Cyclic voltammetric (CV) behavior of Ru–Ti oxide films

As part of the early steps in the characterization of the films, CV data were collected in fresh 5 mol/L NaCl solutions prior to the electrolysis experiments. It is known (1, 2, 22–24) that the CV response of these electrodes reflects the reversible conversion of the Ru sites at the film surface from Ru(II) at the negative end of the scan to Ru(IV) at more positive potentials. The CV behavior at 100 mV/s for oxide electrodes of varying Ru content is shown in Fig. 1 at 20–22°C (solid lines) and at 90°C (dotted lines) in 5 mol/L NaCl, between 0.5 and 1.0 V vs. SCE. It can be seen from Fig. 1 that the magnitude of the CV currents decreases with decreasing Ru content, particularly for the less than 15 at.% Ru oxide films. Also, the effect of temperature on the response is negligible down to 10 at.% Ru, below which increased temperature yields significantly higher currents, especially for the 5 at.% Ru oxide.

Figure 2 (open symbols) shows a plot of the reciprocal of

² B.V. Tilak. Private communication.

Fig. 1. Cyclic voltammograms of Ru–Ti oxide electrodes (2 μm thick) with varying Ru content in 5 mol/L NaCl (pH ca. 4) at 100 mV/s at room temperature (solid lines) and at 90°C (dotted lines).

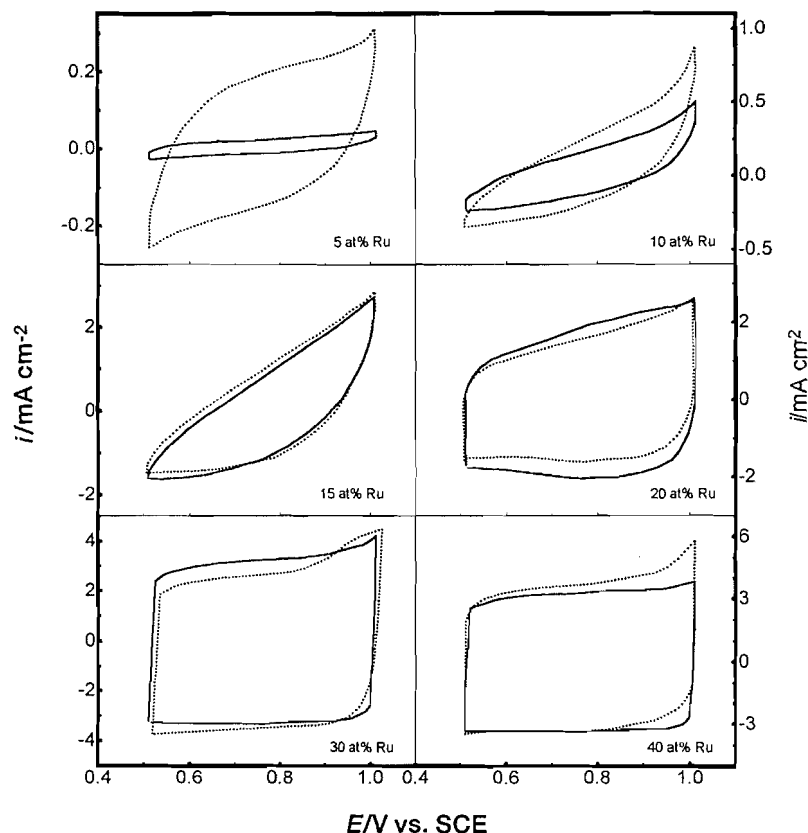
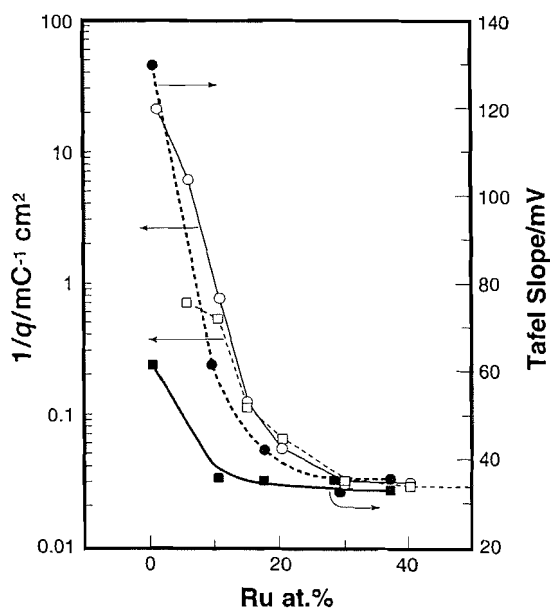


Fig. 2. Relationship of reciprocal CV charge densities (room temperature, open circles; 90°C, open squares) and of the Tafel slope obtained during chlorine evolution (room temperature, closed circles; 90°C, closed squares) on the Ru content for 2 μm thick Ru–Ti oxide films in 5 mol/L NaCl (pH ca. 4).



the logarithm of the integrated charge density (passed in a single anodic scan) as a function of the Ru content of the film. The inverse log of the charge density decreases linearly up to ca. 25 at.% Ru, and then takes on a close to steady-state value at higher Ru compositions. Clearly, the addition of Ru to the Ti oxide film not only results in a proportional increase in the density of surface-active Ru sites, but also leads to other changes in film properties.

Figure 3(a) shows the room temperature CV response for a pure, thermally formed Ti oxide film, demonstrating the very low capacitance of this semiconducting material. Figure 3 (b and c) displays the CV responses for pure Ru oxide films at room temperature and at 90°C, respectively. The higher charges and the more capacitive appearance of the CV response in Figs. 3b and 3c for pure Ru oxide films appears very similar to the CV data for mixed Ru–Ti oxide films of more than 20 at.% Ru, shown in Fig. 1. Clearly, the CV response for Ti oxide (Fig. 3a) is more similar to those of the 5 and 10 at.% Ru films in Fig. 1, suggesting that the more marked effect of temperature in Fig. 1 for these oxides reflects an increase in conductivity.

The effect of film thickness on the CV response of 40 at.% Ru oxide films is shown in Fig. 4. The currents and charge densities are seen to be approximately proportional to the estimated film thicknesses of 0.6 and 2 μm . If the Ru–Ti oxide CV response is proportional to the available surface area, as was reported earlier for thermally formed films (12, 25, 26), then these results suggest that these films are homogeneously

Fig. 3. Cyclic voltammograms in 5 mol/L NaCl (pH ca. 4): (a) thermally formed TiO_2 , formed on Ti at 440°C for 30 min, room temperature; (b) anodically formed RuO_2 on Ru (2 V for 5 min); room temperature; (c) same as (b), but at 90°C.

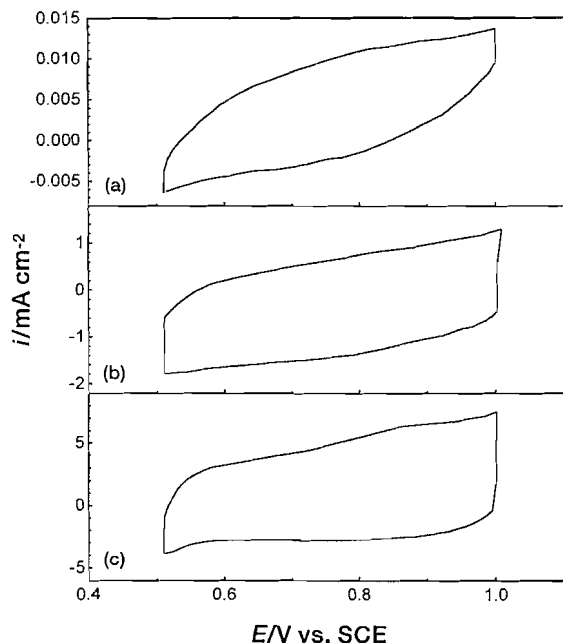
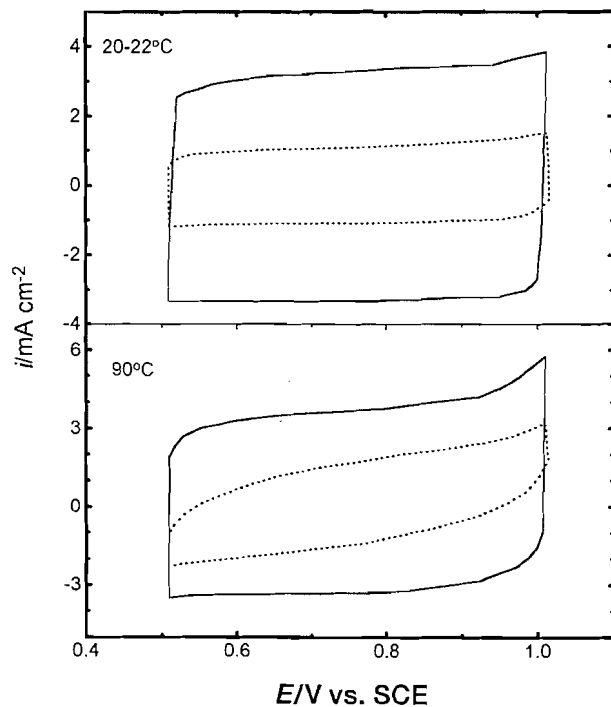
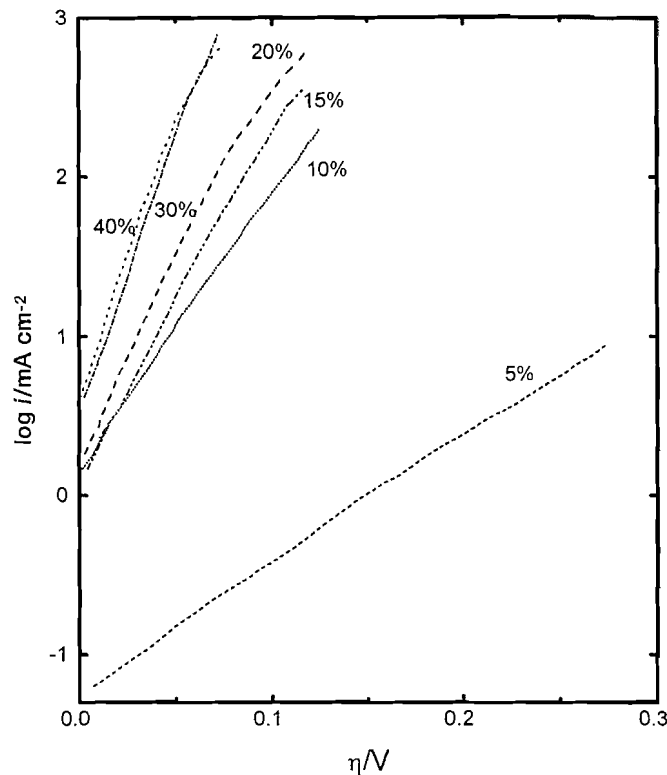


Fig. 4. Cyclic voltammograms of Ru(40 at.%) – Ti oxide electrodes at room temperature and 90°C in 5 mol/L NaCl (pH 3–5) at 100 mV/s; 2 μm thick coatings (solid lines); 0.6 μm coatings (dotted lines).



porous materials and that all of the Ru surface sites are accessible for reaction under these experimental conditions. The research of Burke and O'Neil (13) also concluded that the CV charge is a measure of the true surface area of the oxide film,

Fig. 5. Polarization behavior of Ru–Ti oxide electrodes with varying at.% Ru in 5 mol/L NaCl (pH ca. 4) at room temperature.



and that it is proportional to the Ru content of the film (from 10 to 100 at.% Ru).

3.2 Effect of Ru content of the oxide films on chlorine evolution Tafel plots

The i/E relationship of the chlorine evolution reaction was established after electrolysis had been carried out for a relatively long period of time, such that the solution could be considered to have equilibrated in terms of dissolved chlorine and hypochlorite, at both temperatures studied. In these experiments, the potential was scanned at 1 mV/s from the OCP (1.05 V) to a maximum current of ca. 800 mA cm^2 (potentiostat oscillations occurred during IR compensation at currents higher than this) and then back to the OCP. Figure 5 shows a typical set of Tafel data for the chlorine evolution reaction at freshly formed, 2 μm thick, Ru–Ti oxide films of varying Ru contents at room temperature. Both the Tafel slope and the exchange current density of the reaction are clearly affected by the oxide composition, with the most notable difference being observed for the 5 at.% Ru film. These results are in agreement with those reported earlier (8, 16) for thermally formed Ru–Ti oxide films.

The effect of the Ru content on the Tafel slopes is shown more clearly in Fig. 2 (closed symbols). It is seen that, at room temperature, the Tafel slope increases for oxide films containing less than 25 at.% Ru, while, at 90°C, an effect on the slope is seen only when the Ru content is less than 10 at.%. At high Ru contents, the Tafel slope is in the range of 30–40 mV, while, at low contents, a higher ca. 120 mV slope is seen, in agreement with prior literature reports (8, 16).

Figure 6 shows the exchange current density for the chlo-

Fig. 6. Effect of at.% Ru in Ru-Ti oxide films of 2 μm thickness on exchange current density of chlorine evolution reaction in 5 mol/L NaCl (pH ca. 4) at room temperature (circles) and at 90°C (squares).

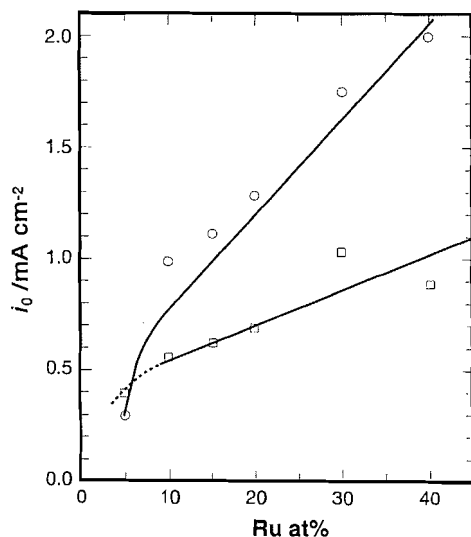
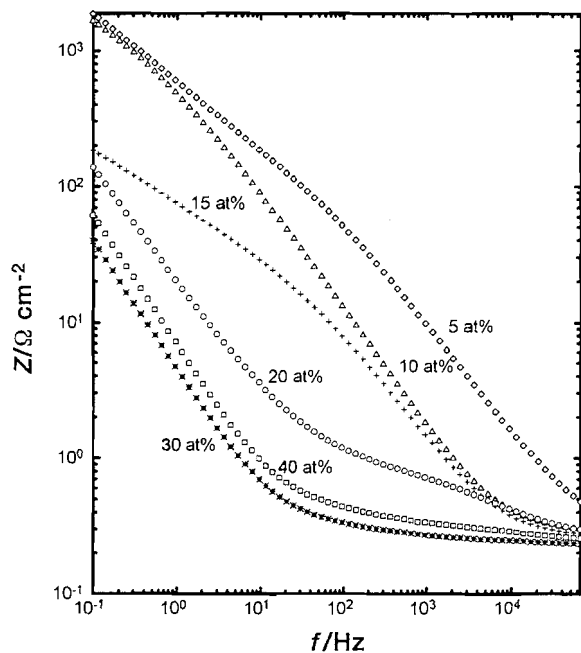


Fig. 7. Frequency dependence of total impedance of Ru-Ti oxide electrodes with different Ru contents in 5 mol/L NaCl (chlorine-free) at room temperature at the OCP.



rine evolution reaction as a function of oxide composition. At both temperatures, the relationship between the exchange current density and the Ru content of the oxide film is linear down to ca. 10 at.% Ru. For the 5 at.% Ru films, the exchange currents are clearly very much reduced. Figure 6 also shows that the exchange current densities at 90°C are lower than the corresponding values at room temperature. This presumably reflects a difference in the nature of the adsorbed surface species participating in the rate-determining step at these two temperatures.

It is widely accepted that the Tafel slope for the chlorine

Fig. 8. Frequency dependence of phase angle of Ru-Ti oxide electrodes with different Ru contents in 5 mol/L NaCl (chlorine-free) at room temperature at the OCP.

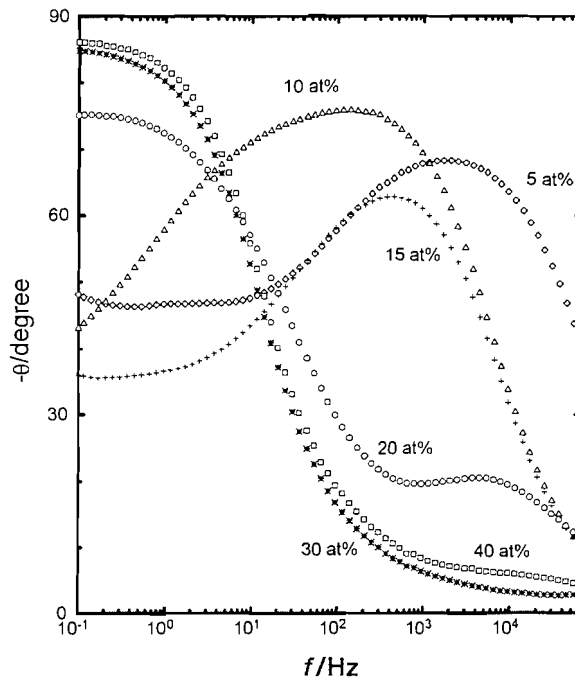
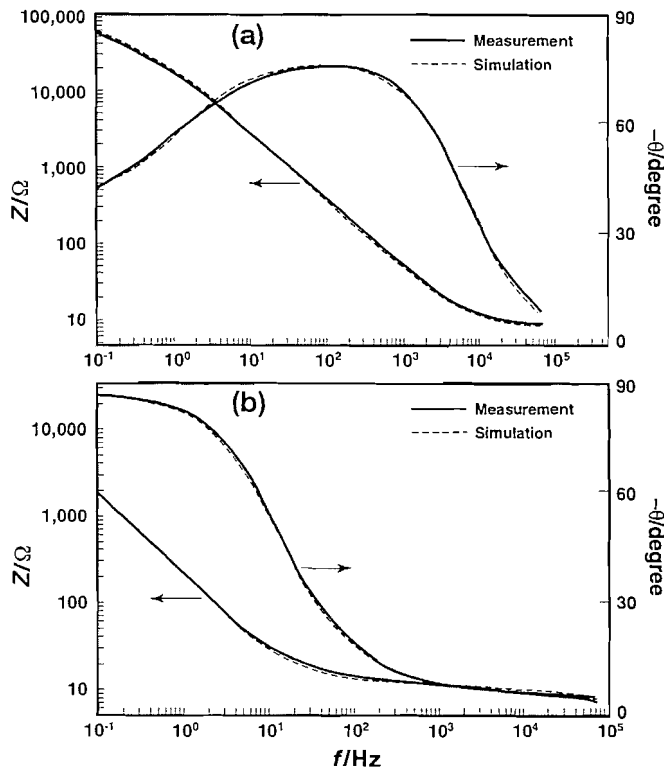


Fig. 9. Comparison of experimental impedance (Z) and phase angle (θ) data with values calculated using the best-fit equivalent circuit parameters in Table 1. (a) 10 at.% Ru; (b) 40 at.% Ru.



evolution reaction should be ca. 40 mV (1, 2), indicative of a slow desorption step. The 30 mV slope seen in Fig. 2 for high Ru contents may indicate the slow diffusion of the product away from the electrode surface, such that it becomes super-

saturated with adsorbed chlorine, or that a rapid discharge reaction is followed by a slow recombination step (2). To explain the increasing Tafel slope with decreasing Ru content, several possibilities can be considered. First, as the Ru site density decreases with lower Ru content, the probability of interaction of a chloride ion with an adsorbed chlorine atom intermediate (expected to yield a 40 mV Tafel slope) is likely to decrease, and therefore the mechanism may change to one in which the discharge reaction is slow (120 mV Tafel slope). The Tafel slopes of between 40 and 120 mV at intermediate Ru contents might then reflect the fact that both of these mechanisms are occurring simultaneously on the surface for films of between 10 and 25 at.% Ru. A second option to explain the data of Fig. 2 is that, at high Ru surface site densities (>25 at.% Ru), the surface coverage of adsorbed chlorine atoms is close to zero, which would yield the expected Tafel slope of ca. 40 mV for this reaction. However, at lower Ru contents, as the reaction rate decreases, it is possible that the surface coverage by adsorbed chlorine atoms increases to unity, which would be consistent with a 120 mV slope. A still more likely possibility is that the experimental Tafel slope reflects not only the mechanism of the chlorine evolution reaction, but also the resistance of the oxide film substrate (27, 28). This would then suggest that the trends in the Tafel slope should be paralleled by similar trends in the oxide resistance. This will be discussed below, based on the impedance results shown.

The exchange current density would be expected to vary linearly with the Ru surface site density, which should be proportional to the Ru content of the film, consistent with what is seen in Fig. 6 down to 10 at.% Ru. The lower value for the 5 at.% film suggests that either some of the Ru sites are no longer accessible or that the oxide surface does not reflect the bulk oxide composition and is behaving anomalously, i.e., more like a poorly conducting Ti oxide film.

3.3 Effect of oxide film Ru content on the ac impedance response

All of the ac impedance data were collected at room temperature in a 5 mol/L NaCl solution. Solution stirring and deaeration were found not to affect the ac response and therefore no attempts were made to remove oxygen or agitate the solution. Most previous ac impedance studies of this system have been carried out in chlorine-saturated solutions near the chlorine-chloride equilibrium potential (29–32), i.e., at ca. 1.05 V vs. SCE. As the emphasis in the present study has been on examining the oxide film properties in the absence of the chlorine evolution reaction, the ac impedance data were gathered primarily at the OCP of the mixed oxide electrodes in solutions containing no dissolved chlorine, i.e., near 0.4 V vs. SCE.

Figures 7 and 8 show the total impedance and phase angle Bode representations for oxide films ranging between 5 and 40 at.% Ru at the oxide OCP in chlorine-free solutions. It is seen that the 20–40 at.% Ru oxides are generally quite similar in their response, and that the biggest change occurs at 15 at.% Ru and lower. This pattern is consistent with the CV data of Fig. 1 and the Tafel slope data in Fig. 2, showing the impact of the oxide properties on the chlorine evolution reaction. The impedance at low frequencies indicates that the resistance of the oxide film is particularly high for the 5–10 at.% Ru films, with the 15 and 20% films exhibiting intermediate resistances, in agreement with prior published results (7). At high frequen-

cies, a resistance value of ca. 6 Ω , corresponding to the solution resistance, is seen in all cases.

The phase angle data in Fig. 8 is particularly interesting in terms of revealing the changing electrical properties of these films with Ru content. Again, the transition in properties is most notable at 15–20 at.% Ru. With decreasing Ru content, it is seen that a second time constant appears at high frequencies, with its phase angle maximum increasing in magnitude and moving to lower frequencies from 20 to 10 at.% Ru in the coating. Interestingly, for the 5 at.% Ru containing Ru–Ti oxide film, the phase angle maximum decreases somewhat, and moves back to higher frequencies, perhaps indicating that the 5% Ru film is significantly different from the others and behaves more like a conventional capacitive oxide material, with the large fraction of TiO₂ likely serving as its ohmic component.

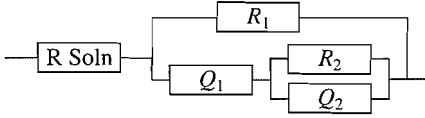
The analogous set of experiments were carried out with these oxide films in a chlorine-saturated solution at 1.05 V. The phase angle data, in particular, displayed several important trends (not shown in a figure) in common with those at the oxide OCP in Fig. 8, namely, that, with decreasing Ru content, a new high-frequency time constant develops, with its phase angle maximum increasing and moving to lower frequencies. The data for the 5 at.% Ru containing Ru–Ti oxide film was again anomalous, in that its high-frequency time constant has moved to higher frequencies.

3.4 Interpretation of impedance data for mixed Ru–Ti oxides

Two approaches were taken in this work to understand and interpret the impedance data, shown in Figures 7 and 8. The first involved identifying the best-fit equivalent circuit (EQC), based on Boukamp's *EQUVCIRC* software, in order to establish the values of the circuit elements. The intention of this work was to then correlate their values with the Tafel and CV data as a function of oxide film composition. The usual guidelines for the selection of the best-fit EQC were followed, i.e., that a minimum number of circuit elements be employed; that, as far as possible, the same circuit is used for all film compositions; and that the χ^2 error, as well as the errors associated with each element, is suitably low (33). Many equivalent circuits were examined, but only that shown in Table 1 obeyed these criteria. Also, this circuit fit well to the impedance data obtained at both the OCP in chlorine-free solutions and at 1.05 V in chlorine-saturated media.

Figure 9 depicts the overlay of the experimental (at the OCP in chlorine-free solutions) and the calculated Bode data, using the EQC shown in Table 1, for the 10 and 40 at.% Ru oxide films, respectively, and shows a high quality of fit over the entire frequency range. The fit for the 5 at.% Ru oxide film was somewhat less satisfactory, again indicating that the properties of this film are quite different from those of the other films, consistent with the apparently anomalous positive shift of the second high-frequency time constant (Fig. 8).

Table 1 gives the values of the circuit elements for the six oxide films at the OCP, based on this EQC. It should be noted that the solution resistance, R_{soln} , was ca. 6 Ω in all of this work, in agreement with the expected electrolyte resistance between the oxide electrode surface and the SCE. R_1 , the parallel resistance, lies between ca. 10^3 and $10^4 \Omega \text{ cm}^{-2}$ in all cases. R_1 is likely to represent the dc leakage current arising

Table 1. Best-fit "equivalent circuit" data.


% Ru	R_1 ($\Omega \text{ cm}^{-2}$)	R_2 ($\Omega \text{ cm}^{-2}$)	Q_1 (mF cm^{-2})	n_1	Q_2 (mF cm^{-2})	n_2
5	4 500	120	0.53	0.70	0.16	0.80
10	3 000	300	0.66	0.87	0.66	0.85
15	300	30	4.50	0.70	1.20	0.79
20	—	0.9	11.66	0.83	18.23	0.50
30	24 000	1.2	26.66	0.95	—	—
40	4 500	0.3	41.66	0.97	—	—

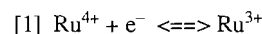
from faradaic reactions involving trace impurities in solution (e.g., the reduction of trace oxygen), which occurs at the OCP (32). As R_1 does not appear to depend on the oxide film properties, its impact on the observations is ignored in the present discussion.

Q_1 and Q_2 represent constant phase elements (CPEs), with n_1 and n_2 reflecting how similar these elements are to a pure capacitor, for which $n = 1$. Notably, both Q_1 and Q_2 increase with the Ru content in the film, with Q_1 likely reflecting the oxide pseudocapacitance and, hence, the number of active Ru sites at the oxide-solution interface. In fact, a rough comparison between these Q_1 values (without converting them to capacitance values through their n values) and the oxide capacitance, estimated from the CV responses in Fig. 1 (current divided by sweep rate), yield very similar pseudocapacitances, confirming this suggestion. The fact that the n_1 values are so close to unity for the 30 and 40 at.% Ru oxide films indicates the formation of nearly perfectly capacitive films, whereas the decreasing n_1 values with decreasing Ru content show the development of nonideality in the capacitive characteristics, probably due to decreasing matrix conductivity (34).

The R_2 values also show an interesting trend with increasing Ru content of the film, decreasing from ca. 10^2 to ca. $0.5 \Omega \text{ cm}^{-2}$, consistent with the expected change in film conductivity. The Q_2 value also increases with increasing Ru content. For the 30 and 40 at.% Ru films, the best-fit Q_2 values were unreasonably high, up to 1 F cm^{-2} (larger than any possible capacitance in the system). However, as their n values were very low, less than 0.2, this indicates that the second CPE is not a valid part of the EQC, and that Q_2 should be replaced by a resistor (33).

Overall, it should be stated that, while the data could be best accounted for by the equivalent circuit shown in Table 1, the circuit itself cannot be said to have any absolute physical meaning. However, it is interesting that, even when the data were fit (although with higher error) to several other equivalent circuits containing the same or almost the same number of elements, the Q and R values were very similar to the R_2 and Q_1 values in Table 1. This strongly suggests that these values do, in fact, accurately reflect the electrical characteristics of these oxide films and were therefore used in the treatment below.

The second approach used in the present work to understand and interpret the impedance response of these Ru-Ti oxide films follows an earlier mechanistic description (35) employed to explain the response of Ru oxide based capacitors to small signal ac perturbations. Attempts were made here to verify this mechanistic approach by comparing the calculated impedance data (specifically the phase angle Bode plots) with those obtained experimentally. The equivalent circuit for a simple one-electron, activation-controlled surface redox process occurring on a planar Ru-Ti oxide surface at the OCP (reaction [1]),



was shown (33) to be represented by the circuit in Fig. 10a. The double layer capacitance (C_d) is located in parallel with the charge transfer resistance (R_t) and the film pseudocapacitance (C_ϕ), which are in series with each other.

The impedance of the same reaction [1], but occurring in a porous matrix structure, was shown (35) to be represented by the following relationship:

$$[2] \quad Z(p) = \frac{1}{\sigma' S} \left(\frac{\coth(ml)}{m} \right)$$

where

$$[3] \quad \sigma' = \frac{\sigma A}{S}$$

and

$$[4] \quad m = \sqrt{\frac{1}{\sigma'} \left(p C_d + \frac{p C_\phi}{(p C_\phi R + 1)} \right)}$$

$Z(p)$ refers to the generalized impedance, p to the Laplace transform variable in the Heaviside notation, σ to the specific conductance of the solution phase ($\Omega^{-1} \text{ cm}^{-1}$), A to the cross-sectional area (cm^2), l to the pore length, R to the sum of the charge transfer and film matrix resistance, and S to the surface

Fig. 10. Theoretical equivalent circuit for an activation-controlled surface redox reaction reaction [1]) occurring (a) at a planar surface; (b) at a porous electrode.

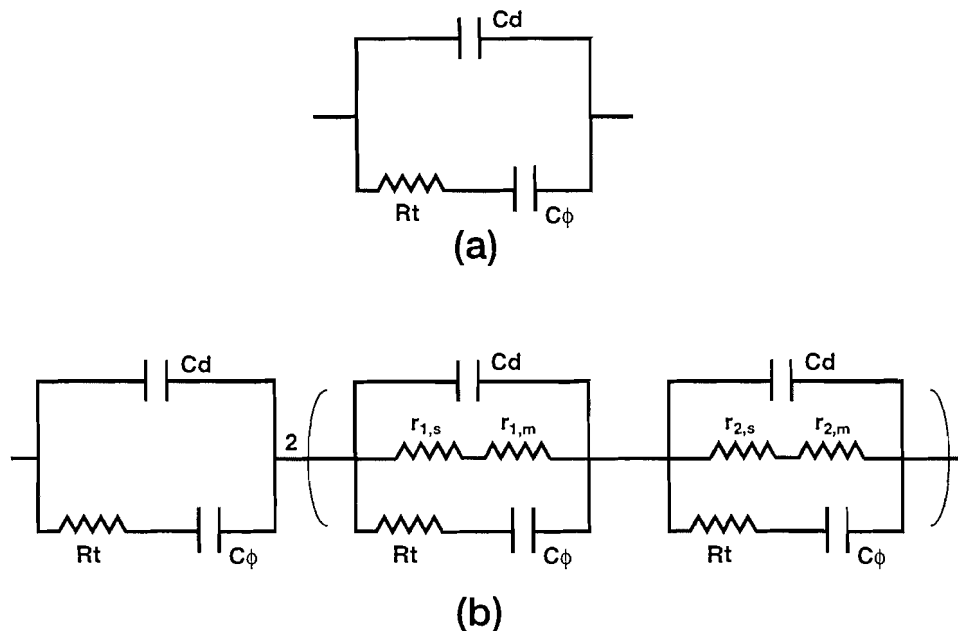
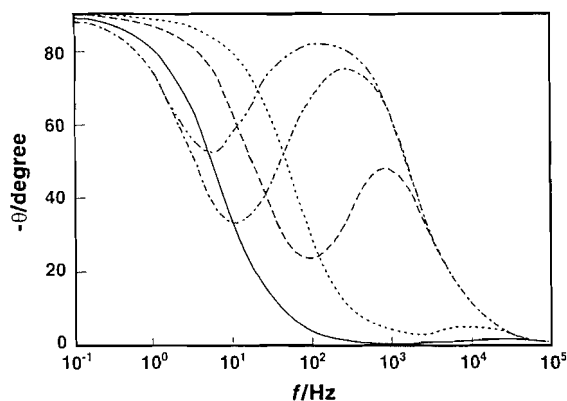


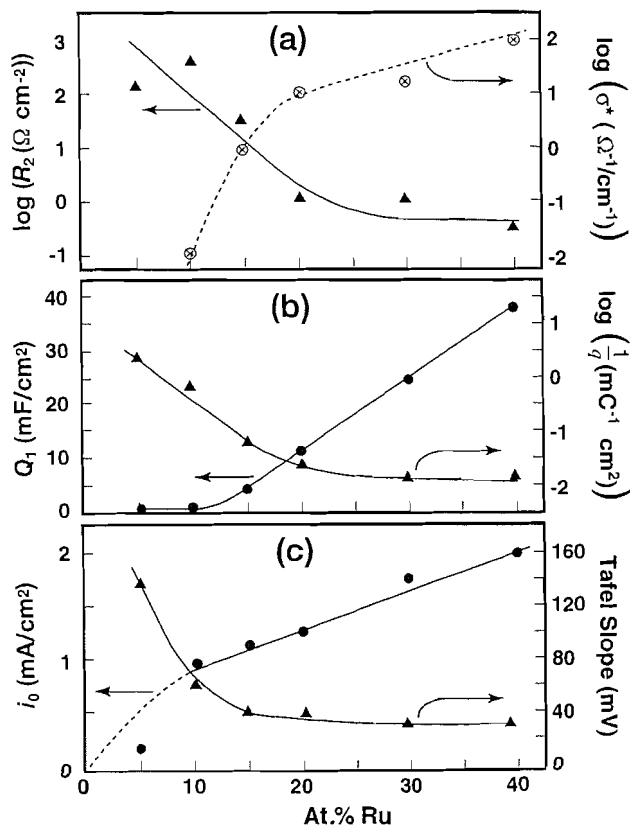
Fig. 11. Phase angle vs. frequency plots, calculated using eq. [2]. $C_\phi = 30 \text{ mF}$, $R = 0.3 \Omega$ (—). $C_\phi = 3 \text{ mF}$; $R = 1 \Omega$ (.....). $C_\phi = 1.5 \text{ mF}$; $R = 30 \Omega$ (-----). $C_\phi = 1 \text{ mF}$; $R = 300 \Omega$ (- - - - -). $C_\phi = 0.3 \text{ mF}$; $R = 1300 \Omega$ (.....).



area of the porous matrix per unit film thickness. The capacitances and resistances are both defined per unit surface area; the solution resistance in the pores of the film is accounted for in the calculation of σ .

The equivalent circuit derived from eq. [2] is shown in Fig. 10b. The outer surface of the oxide film is represented by the same circuit as shown in Fig. 10a for a planar electrode, while charge transport in the pores of the film matrix yields the transmission line component, with only two units (of a possible n units) of the transmission line shown in parentheses in Fig. 10b. The resistance of the oxide matrix, r_m , has been added in the present treatment, and appears (36) in series with the pore solution resistance, r_s , in Fig. 10b. The separation of R_t , r_m , and r_s is difficult, if not impossible, as these elements are lumped together with the capacitors (37), constituting the overall system resistance.

Fig. 12. Variations of electrochemical characteristics of Ru-Ti oxide films as a function of at.% Ru. (a) R_2 and $\log \sigma$. (b) Q_1 (Table 1) and $\log (1/q)$ (Fig. 2). (c) i_0 and Tafel slope (from Figs. 2 and 6) at room temperature.



Phase angle calculations were performed by inserting the R_t (same as R_2 in Table 1), and C_ϕ (same as Q_1 in Table 1) values, obtained at the OCP (in chlorine-free solutions) from the best-fit EQC method, into eq. [2]. R_s was taken to be 5Ω and C_d was set at $100 \mu\text{F cm}^{-2}$, which appears reasonable, based on the discussion presented in ref. 1. The calculated results shown in Fig. 11 reveal the essential features of the experimental phase angle Bode plots in Fig. 8. It is seen that, as the sum of the charge transfer resistance and the oxide matrix resistance increases, a peak develops in the high-frequency region of the Bode plot, moving to lower frequencies as the at.% Ru in the coating decreases. The peculiar experimental result for the 5 at.% Ru films in Fig. 8 could not be obtained by this calculation, perhaps as a result of the very high resistivity of this film and the likely existence of a TiO_2 dielectric capacitance in this case.

It is notable that this mechanistic derivation of the impedance, based on the assumption of the activation-controlled reaction of surface Ru sites occurring throughout a porous matrix, and employing the R and C values obtained from the EQC fitting procedure, leads to a very similar phase angle response as seen experimentally (except for the 5 at.% film). This lends support to the validity of the heuristic EQC approach, the suggested mechanism of the reaction, as well as the porous character of these films. This also confirms the data in Table 1, showing the development of matrix resistivity and a loss in pseudocapacitance with decreasing Ru content of the film. The most significant increase in the resistivity occurs below about 20 at.% Ru, in agreement with the conductivity data published in the literature (4, 7, 9, 34).

Figure 12 correlates the kinetic results obtained here for the chlorine evolution reaction and the impedance data at the oxide OCP, obtained from EQC fitting. It is interesting to note that, while the exchange current density for the chlorine evolution reaction shows a linear dependence on the Ru content (Fig. 12c) for films of more than 5 at.% Ru, this behavior is not revealed in either the Tafel slope variations (Fig. 12c) or in the Q_1 and R_2 parameters deduced from the EQC in Table 1 (Figs. 12a and 12b). This is to be anticipated, as the magnitude of Tafel slope and the impedance of the system are both a function of the mechanism of the reactions involved at the OCP or during the course of the chlorine evolution reaction, the mechanism being controlled not only by the number of active Ru sites in the film, but also dictated by the matrix resistivity. It should also be noted that the variations in R_2 , Q_1 , and $1/q$ change significantly in the range of 10–20 at.% Ru, similar to the change in the Ru–Ti oxide conductivity (σ'), determined independently (4, 7, 9, 34).

The results presented in this investigation show clearly that the signature of the developing matrix resistance with decreasing Ru content of the oxide film is revealed more dominantly in the phase angle Bode plots than in either the Tafel slopes or the overall impedance plots, although the latter parameters are also affected by the coating resistance. It will be shown in a forthcoming communication that, in practice, the performance characteristics of electrodes that have become electrochemically inactive after long times of electrolysis closely resemble those of freshly formed oxides of low Ru content. This implies that anode deactivation results from the selective loss of Ru from the oxide film with time of chlorine evolution and hence a markedly increased increase in resistance, as well as a loss in active surface sites.

Acknowledgements

Grateful acknowledgement is made to the Natural Sciences and Engineering Research Council of Canada for partial support of this work, and to Dr. Petr Vanýsek, Northern Illinois University, for helpful discussions.

References

1. S. Trasatti. *In* The electrochemistry of novel materials. *Edited by* J. Lipkowski and P.N. Ross. VCH Publishers, New York. 1994. Chap. 5, p. 207.
2. B.E. Conway and B.V. Tilak. *Adv. Catal.* **38**, 1 (1992).
3. S. Trasatti. *Electrochim. Acta*, **32**, 369 (1987).
4. W.A. Gerrard and B.C.H. Steele. *J. Appl. Electrochem.* **8**, 417 (1978).
5. F. Hine, M. Yasuda, and T. Yoshida. *J. Electrochem. Soc.* **124**, 500 (1977).
6. L.D. Burke, O.J. Murphy, and J.F. O'Neill. *J. Electroanal. Chem.* **81**, 391 (1977).
7. E.K. Spasskaya, Y.B. Makarychev, A.A. Yakovleva, and L.M. Yakimenko. *Soviet Electrochem.* **13**, 327 (1977).
8. M.D. Spasojevic, N.V. Krstajic, and M.M. Jaksic. *J. Res. Inst. Catal. Hokkaido Univ.* **31**, 77 (1983).
9. P.H. Duvinéaud and A. Coussement. *J. Solid State Chem.* **52**, 22 (1984).
10. K. Doblhofer, M. Metikos, Z. Ogumi, and H. Gerischer. *Ber. Bunsen-Ges. Phys. Chem.* **82**, 1046 (1978).
11. L.D. Burke and O.J. Murphy. *J. Electroanal. Chem.* **96**, 19 (1979).
12. L.D. Burke and O.J. Murphy. *J. Electroanal. Chem.* **112**, 39 (1980).
13. L.D. Burke and J.F. O'Neil. *J. Electroanal. Chem.* **101**, 431 (1979).
14. D.T. Shieh and B.J. Hwang. *Electrochim. Acta*, **38**, 2239 (1993).
15. E.W. Tsai and K. Rajeshwar. *Electrochim. Acta*, **36**, 27 (1991).
16. A.T. Kuhn and C.J. Mortimer. *J. Electrochem. Soc.* **120**, 231 (1973).
17. C.E. Vallet, D.E. Heatherly, and C.W. White. *J. Electrochem. Soc.* **137**, 579 (1990).
18. C.E. Vallet. *J. Electrochem. Soc.* **138**, 1234 (1991).
19. C.A. Gervasi and J.R. Vilche. *Electrochim. Acta*, **37**, 1389 (1992).
20. S.G. Real, J.R. Vilche, and A.J. Arvia. *J. Electroanal. Chem.* **341**, 181 (1992).
21. E.B. Castro, S.G. Real, R.H. Milocco, and J.R. Vilche. *Electrochim. Acta*, **36**, 117 (1991).
22. S. Trasatti and G. Buzzanca. *J. Electroanal. Chem.* **29**, App 1 (1971).
23. V.I. Birss, R. Meyers, H. Angerstein-Kozłowska, and B.E. Conway. *J. Electrochem. Soc.* **131**, 1502 (1984).
24. S. Ardizzone, G. Fregonara, and S. Trasatti. *Electrochim. Acta*, **35**, 263 (1990).
25. D. Mitchell, D.A.J. Rand, and R. Woods. *J. Electroanal. Chem.* **89**, 11 (1978).
26. L.D. Burke and E.J.M. O'Sullivan. *J. Electroanal. Chem.* **117**, 155 (1989).
27. S.K. Rangarajan, M.J. Dignam, and B.E. Conway. *Can. J. Chem.* **45**, 422 (1967).
28. B.V. Tilak, S. Venkatesh, and S.K. Rangarajan. *J. Electrochem. Soc.* **136**, 1977 (1989).
29. I.R. Burrows, D.A. Denton, and J.A. Harrison. *Electrochim. Acta*, **23**, 493 (1978).
30. D.A. Denton, J.A. Harrison, and R.I. Knowles. *Electrochim. Acta*, **24**, 521 (1979).

31. D.A. Denton, J.A. Harrison, and R.I. Knowles. *Electrochim. Acta*, **25**, 1147 (1980).
32. J.A. Harrison, D.L. Caldwell, and R.E. White. *Electrochim. Acta*, **29**, 203 (1984).
33. A.J. Zhang, V.I. Birss, and P. Vanýsek. *J. Electroanal. Chem.* **378**, 63 (1994).
34. C.E. Vallet. *J. Electrochem. Soc.* **138**, 1234 (1991).
35. B.V. Tilak, C.-P. Chen, and S.K. Rangarajan. *J. Electroanal. Chem.* **324**, 405 (1992); **356**, 319 (1993).
36. B. Pillay and J. Newman. *J. Electrochem. Soc.* **143**, 1806 (1996).
37. S.K. Rangarajan. *J. Electroanal. Chem.* **22**, 89 (1969); **41**, 459 (1973).